Pergamon

0042-6989(95)00286-3

Vision Res., Vol. 36, No. 15, pp. 2351–2367, 1996

Printed in Great Britain
0042-6989/96 $15.00 + 0.00

Illumination, Shading and the Perception of Local Orientation

PASCAL MAMASSIAN,* DANIEL KERSTEN*†

Received 25 January 1995; in revised form 27 July 1995; in final form 23 October 1995

We investigated the perception of local surface orientation on a simple smooth object, under several different illumination conditions. The perceived local orientation was determined for several points on the surface and quantified as slant and tilt of the local tangent plane. We found an underestimation of the perceived slant and a larger variance for the perceived tilt than for the perceived slant. We found also that subjects were less biased at estimating the surface orientation when the shape was locally egg-shaped rather than saddle-shaped or cylindrical. In order to investigate the relationship between perceived shape and light source direction, we developed a method to compute the light source direction most consistent with an observer's settings. Also we compared human errors with those of an "ideal observer" which makes explicit assumptions about the illuminations, shapes and materials in its world. From converging evidence based on (i) the light direction most consistent with the observer's settings; (ii) a supplementary experiment where the object is displayed as a silhouette, and (iii) the computer simulations of the ideal observer, we conclude that the observers used the occluding contour of the object rather than shading to estimate the local surface orientation. Copyright © 1996 Elsevier Science Ltd.

Shape from shading Surface reconstruction Surface orientation Occluding contour

INTRODUCTION

From the reflection of light on surfaces, patterns of shading are produced in relation to the shape of the surfaces. The apparent sense of relief rendered by shading is at the origin of the Renaissance drawing school known as chiaroscuro. Leonardo da Vinci, and later the Flemish masters, developed the school by emphasizing the interplay between light and shade in their paintings. The fascination with shading seems to have reached a pinnacle with drawings such as those of Georges Seurat (*cf.* Franz & Growe, 1984), in which a visual scene is rendered without any salient contour.

In spite of its apparent significance to the three-dimensional quality of a surface, shading as a cue to shape has produced a less enthusiastic response from vision scientists. This general mistrust towards the shading cue is a consequence of both theoretical and empirical results. Theoretically, shape from shading is strongly underconstrained (Horn & Brooks, 1989). Indeed, the illuminant intensity, the surface material and the surface orientation all contribute to the light reflected from the surface. These three scene attributes are confounded in a single observable variable: the intensity of the image at each point. Empirically, the interpretation of a shaded image is often ambiguous. For instance, concave objects can be perceived as convex by turning the image upside-down (Gibson, 1950) and shaded surfaces can appear to change shape when their contours are altered (Ramachandran, 1988).

In the face of this discrepancy between our intuitive sense and rational knowledge, we have been interested in the accuracy with which the shape of a simple shaded object was perceived. The organization of the present paper is as follows. In the next section, we review some relevant literature and motivate our work. We then describe the main psychophysical experiment of the paper, in which observers performed a local orientation task. The results of this experiment are further analyzed along three lines. Firstly, we test the influence of the illumination condition by computing the light source direction which is the most consistent with the observers settings, and by comparing this "implicit" light source direction with the actual direction. Secondly, we study the contribution of the information carried by the occluding contour by replicating the experiment, but displaying only the silhouette of the object. Finally, we look at the paucity of information contained in our stimulus by comparing the psychophysical results to that of a shape-from-shading algorithm confronted with a similar task. We conclude the paper with a summary of our results.

* Department of Psychology, University of Minnesota, Minneapolis, MN 55455, U.S.A.

† To whom all correspondence should be addressed at: N218 Elliott Hall, 75 East River Rd, Minneapolis, MN 55455, U.S.A. [*Email* kersten@mach.psych.umn.edu; *Fax* +1-612-626-2079].

PREVIOUS WORK

How can one investigate the effect of shading on shape perception? Use of a global task, such as measuring the "three-dimensional appearance" of the object (Cavanagh & Leclerc, 1989), is often too coarse an approach. More local tasks, therefore, became the favored paradigms, focusing either on the local depth, orientation, or solid shape. Firstly, the study of perceived depth has led to the conclusion that shading was a weaker cue for shape than any other cue in the image (Bülthoff & Mallot, 1988; Todd & Reichel, 1989). However, this result can be attributed to the fact that shading is not a depth cue *per se*; depth information must be obtained by integration of surface orientation, a procedure which is very sensitive to noise. Secondly, the local surface orientation was investigated by directly asking the observer to evaluate the slant and tilt in degrees (Mingolla & Todd, 1986), or by projecting a small gauge figure on the picture of a shaded object (Koenderink *et al.*, 1992). These studies demonstrated that such a task could be repeated with little variability, but unfortunately the error in terms of slant and tilt was not reported. Thirdly, perceived local solid shape has been estimated from its two components, which describe how the surface is curved and how much it is curved (Koenderink, 1990; Mamassian *et al.*, 1996). Regarding the first component, one finds a bias to perceive small quadratic shapes as elliptic convex (Erens *et al.*, 1993); regarding the second component, a shaded cylinder appears flatter than it actually is (Todd & Mingolla, 1983), although a relatively small Weber fraction was found in a curvature discrimination task (Johnston & Passmore, 1994a).

Apart from the explicit recovery of shape from shading, a related problem is concerned with the importance of the illumination condition for the interpretation of a scene. The interest in this problem came from the crater illusion, the phenomenon according to which a pictured object can appear either convex or concave, simply by turning the picture upside-down (Brewster, 1826). The issue behind this first series of studies is whether the visual system assumes that the light is coming from above (Gibson, 1950; Yonas *et al.*, 1979; Berbaum *et al.*, 1984; Ramachandran, 1988). A second series of studies focused on how well people can estimate the direction of illumination in a scene. When asked to report explicitly where the light source was, observers appeared to be very accurate (Pentland, 1982; Todd & Mingolla, 1983). Unfortunately, this conclusion was obtained with spherical and cylindrical objects, for which the direction of illumination can be computed easily from the image. A later study found much poorer performance and, importantly, no correlation was found between this illumination estimation task and a local surface orientation task on the same scene (Mingolla & Todd, 1986).

As we have just remarked, the choice of an inappropriate surface to study can lead to some erroneous conclusions. For instance, the isophotes on a cylinder are always oriented along its axis (*cf.* Todd & Mingolla, 1983) and an elliptic paraboloid will almost always look like a step luminance edge (*cf.* Lehky & Sejnowski, 1990). It seems judicious, therefore, to avoid choosing such objects if anything general about shape from shading is to be stated. Another important factor to consider is the extent of the surface seen by the observer. While very small patches are highly ambiguous if described by shading only (Erens *et al.*, 1993), displaying the whole object will provide another piece of information for the object's shape at the occluding contour.

In summary of these previous studies on shape from shading, it appears that local judgments can be done consistently (small variability), but quite inaccurately (large bias). Unfortunately, because of the set of objects used, neither the effect of the intrinsic shape of the object nor the influence of the illumination condition on the observers' judgments could be addressed genuinely. In our attempt to approach these issues, we chose a croissant-shaped object, which is the simplest, non-trivial smooth object in the sense that its surface includes all local solid shapes (i.e. elliptic, parabolic and hyperbolic points). In contrast to Koenderink *et al.* (1992), who used the picture of a surface, we rendered a computer three-dimensional model of the croissant-shaped object. Computer rendering has the disadvantages of lacking aspects of realism, since a complete model for the illumination of a common surface should theoretically take into account the complex material properties of that surface (*cf.* Oren & Nayar, 1995). On the other hand, computer rendering provided us with a comparison of human settings with both the actual three-dimensional representation of the object and the surface estimated by an ideal observer. Finally, the object always had the same occluding contour, but was illuminated by a single light source whose position was sometimes chosen to be atypical, such as below or behind the object.

EXPERIMENT I: LAMBERTIAN SHADING

Methods

Subjects. Three subjects, naive to the purposes of the experiment, participated in this first study. Two of the observers (WB and SH) were graduate students familiar with computer-generated displays, although only WB was a trained psychophysical observer. The last observer (CM) was an undergraduate student, paid for her time spent on the experiment, and unfamiliar with psychophysical procedures. All observers had normal or corrected-to-normal vision.

Apparatus. A shaded object was simulated using a graphics computer (a Silicon Graphics 4D35 workstation). The object was displayed on a high-resolution (1280×1024 pixels) 19 inch color monitor. The pixel brightness was quantized to 8 bits, providing a maximum of 256 different gray levels. The screen was gamma-corrected to have a linear relationship between the gray-level values from the color-map and the displayed pixel brightness. After correction, the brightness varied from 0.26 to 110 cd/m^2. A reduction screen was placed between the monitor and the observer, so that the display

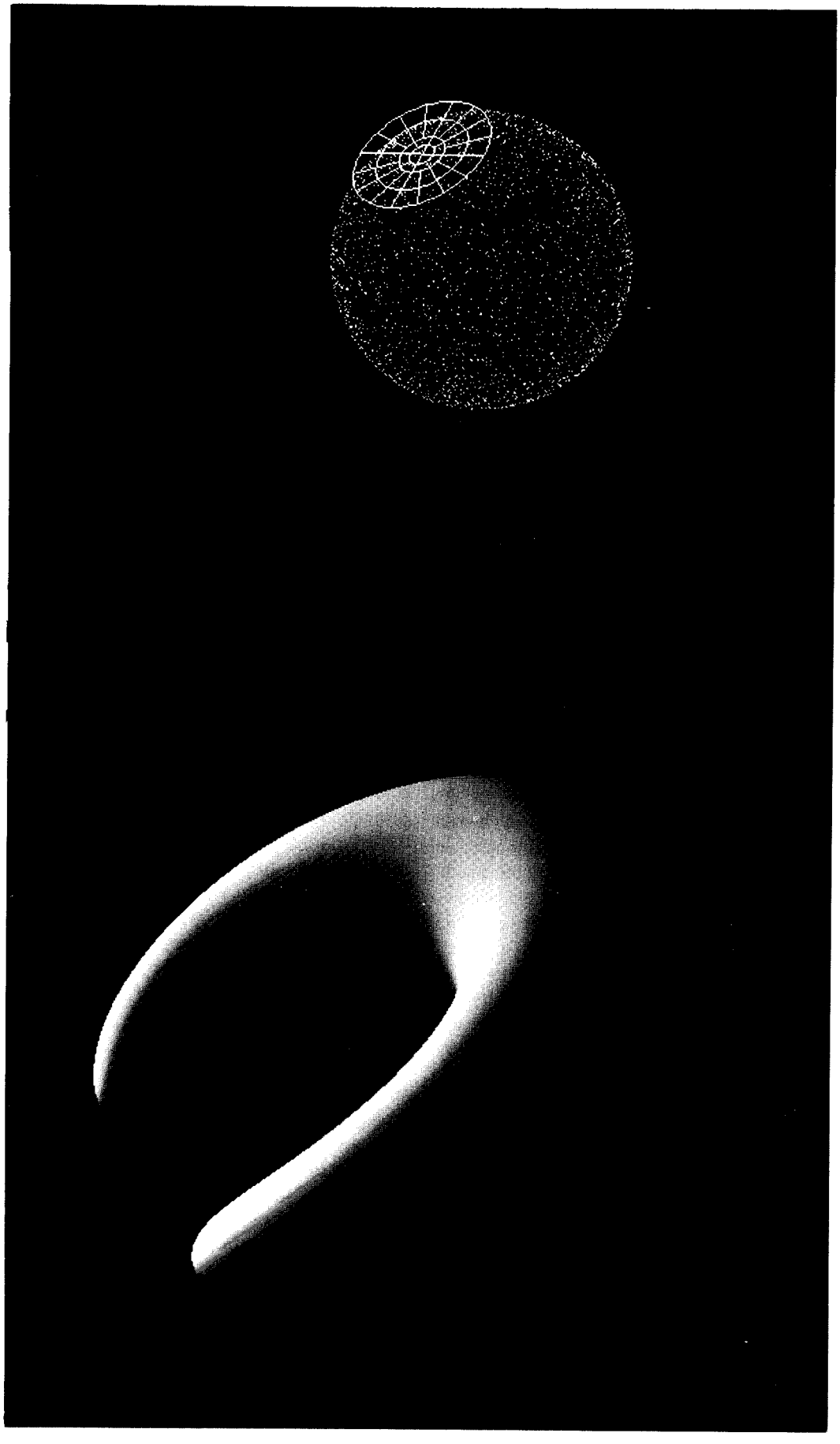

FIGURE 1. The stimulus was a shaded croissant-shaped object. Observers had to match the local orientation of the surface at one point to the orientation of a probe presented on the side of the object.

could be seen only through a small aperture which was out of focus for the observer. Subjects sat in an otherwise dark room, with their head resting on a chin-rest. Viewing was monocular (the other eye covered by an eye-patch) and the viewing distance was 50 cm.

Stimulus. One goal of this study was to look at the effect of the local surface structure on the perceived shape. For this purpose, we needed an object which contained all three qualitatively different points existing on a smooth surface, namely elliptic (locally egg-shaped), parabolic (locally cylindrical) and hyperbolic (locally saddle-shaped). The object chosen was croissant-shaped (Fig. 1), obtained from bending the long axis of an ellipsoid of revolution along a circular arc. The size of the ellipsoid before bending was 48 mm in diameter (circular cross-section) and 120 mm in length, and the circular arc had a radius of 48 mm. The croissant was then oriented in the following way: starting with the canonical orientation, where its two extremities were on top and within the sagittal plane, the croissant was rotated leftwards about the vertical axis by 30 deg and then counterclockwise in the image plane by 30 deg. The object was always viewed from this non-accidental viewpoint, and subtended 11 by 13 deg of visual angle. Before each trial, the whole croissant was translated in the image plane, so as to display the point at which the measurement was made at the center of the screen.

The shading on the croissant was computed directly from Lambert's cosine law. The intensity of the light source and the albedo of the surface were chosen so that the brightest points on the surface (facing the light source) were rendered using the highest value of the color-map (110 cd/m^2). Since a simple Lambertian model was used, there were no specular highlights and no ambient illumination (the attached shadows were black, i.e. the lowest entry of the color-map). The light sources and the object pose were chosen so as to avoid any visible cast shadow. The shape was simulated as a three-dimensional triangular mesh, two vertices being separated at most by about 3 pixels. The computed shading value was applied at each vertex and linearly interpolated following the Gouraud procedure (Foley *et al.*, 1990). The shaded croissant was displayed on a dark gray background (7.1 cd/m^2).

To report perceived surface orientation, observers were asked to use a probe consisting of a simulated tangent plane on a sphere (Fig. 1). The sphere was composed of 2000 visible white dots, drawn from a uniform distribution over its surface. The simulated tangent plane was represented using four concentric circles. The probe, whose diameter subtended 6 deg of visual angle, was presented 12 deg to the side of the croissant. Orthographic projection was used to display both the croissant and the probe on the monitor, so that the orientation of the tangent plane and the local orientation on the surface of the croissant could be directly compared. This comparison assumed that the observer was making his judgment in a world-centered frame of reference.

Design. Twelve points were selected from each of the three local solid *shape* categories (elliptic, parabolic and hyperbolic), providing a total of 36 different measurement points. The local surface orientation at the measurement points is fully described by the slant and tilt of the plane tangent to the surface at one point. Following the usual convention, slant is the angle between the line of sight and the surface normal, while tilt is the angle in the image plane between the projection of the normal in the image and the rightwards horizontal direction. The measurement points were matched according to their *displayed slants*, from 10 to 65 deg in steps of 5 deg (*cf.* Appendix A). To enable the comparison between local solid shapes, the tilts were also matched (within 30 deg) for a given displayed slant (Appendix A). In addition to these shape and slant factors, we used four *lighting* conditions. The light source was located at infinity either at the viewpoint (i.e. at zero slant), above the croissant [(*slant*, *tilt*) = (35 deg, 120 deg)], below it [(*slant*, *tilt*) = (65 deg, −25 deg)], or behind it [(*slant*, *tilt*) = (105 deg, 60 deg)].

The subjects had to match the simulated tangent plane on the textured sphere to the perceived orientation of the surface at a designated point. To do so, they could drag the simulated tangent plane over the sphere using the computer mouse. Perceived slant and tilt were recorded in this way for each trial. After each trial, the object disappeared for 1 sec until the next trial.

We did not overlay the probe disc over the object (as did Koenderink *et al.*, 1992) for the following reasons. If the disc was overlayed to simulate the tangent plane to the surface, it would "slice" the surface at hyperbolic points. Moreover, the outline of the disc (an ellipse in projection) could interfere with the perception of the underlying local solid shape of the surface; indeed, a slice of the surface parallel to the tangent plane and directly below it is elliptic (resp. hyperbolic) if the surface is locally elliptic (resp. hyperbolic) at that point (*cf.* the Dupin indicatrix in, for example, do Carmo, 1976).

The experiment followed a randomized blocked design, with the illumination condition as the blocked factor (four levels), and eight repeated measures for the $12 \times 3 = 36$ measurement points. Each of the eight sessions was preceded by 12 practice trials on a shaded sphere (in lieu of the croissant), whose diameter extended 8 deg of visual angle. During these practice trials, feedback was provided to reduce as far as possible the biases introduced by the probe itself. Feedback was given to the observers by superimposing on the textured sphere the correct tangent orientation, using a different color than the one used for the displaceable tangent probe.

Results and discussion

For the analysis of this experiment, we first describe the errors (both variability and bias) for both the slant and tilt variables. Then we consider the influence of the local solid shape and the illumination condition. Due to experimental errors, eight trials were omitted for subject CM and 17 for SH, out of a total of 1152 trials for each subject.

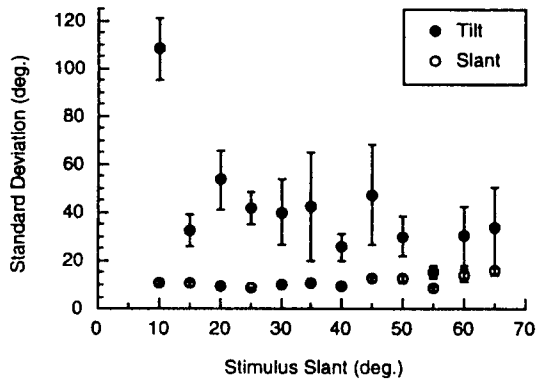

FIGURE 2. The SD for the perceived slant was smaller than the one for perceived tilt. Error bars show SDs of the mean across subjects (standard errors were smaller than symbol size for slant).

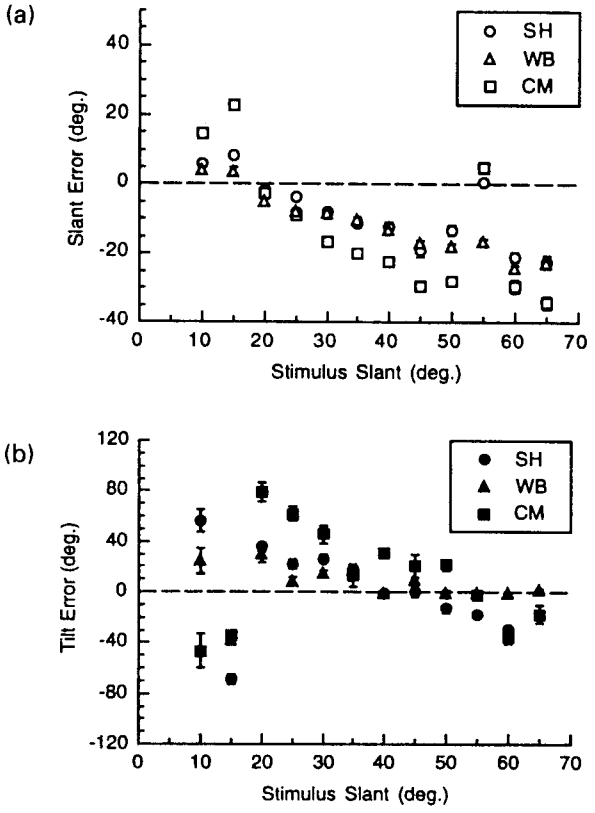

FIGURE 3. Both slant (a) and tilt (b) errors were decreasing functions of the displayed slant (slant at the measurement point). Each plot shows the performance of all three observers.

Slant and tilt variance. The variance of the measurements is an index of the reproducibility of the observers' settings. Since the tilt is not defined when the slant is null, we expected a larger variance for small displayed slants. This was indeed the case (Fig. 2), but we note that for displayed slants strictly larger than 20 deg, the variance of the perceived tilt remained roughly constant. In order to fulfill the variance independence requirement in the forthcoming ANOVA, displayed slants thus were restricted to angles larger than 20 deg for the analysis of the perceived tilt. Similarly, the variance of the perceived slant was constant throughout the range of displayed slants used in the experiment. This independence of the perceived slant variance from the displayed slant speaks in favor of the slant angle (as opposed to its cosine or tangent) for the coding of surface orientation (Stevens, 1983).

Standard deviations for the perceived slant were 13.3 deg (observer WB), 21.8 deg (CM) and 15.0 deg (SH). Standard deviations for the perceived tilt (for displayed slants larger than 20 deg) were in comparison much larger: 21.3 deg (WB), 67.6 deg (CM) and 32.5 deg (SH). A potential interpretation of this result is that the visual system uses the same resolution for both slant and tilt (for instance 1 part in 100), but since tilt varies over a broader range than slant, the accuracy for tilt is necessarily poorer.

While we found a larger variance for tilt than for slant, Koenderink *et al.* (1992, their Fig. 7) found exactly the opposite. In contrast to our experiment, this latter study used a somewhat more complex stimulus and a different probe, although none of these methodological differences seems to provide a convincing explanation for the opposite results.

Slant and tilt errors. We ran a multivariate analysis of variance on the data collected from each subject. To be able to compare our two dependent variables, we chose them to be the slant and tilt errors, instead of just the perceived slant and tilt. The three independent variables were the light source position (four levels), the displayed slant of the measurement point (12 and nine levels for slant and tilt, respectively) and the shape characteristic sign of the point (three levels); each condition was repeated eight times per subject. Since the light source position was blocked, no interaction effect could be computed from this factor.

When perceived slant was plotted against displayed slant, we found an underestimate of the perceived slant for slant larger than 20 deg and an overestimate under this value [Fig. 3(a)]. This effect was very robust and explained most of the variance of the settings for the three observers: $F(11,1113) = 102.4$ ($P < 0.001$) for observer WB, $F(11,1105) = 310.0$ ($P < 0.001$) for CM, and $F(11,1096) = 112.9$ ($P < 0.001$) for SH. The underestimate bias on the slant error increased with the displayed slant and could be well accounted for by a linear model. Calling b the slope of the slant error, we found $b = -0.49$ with a Pearson's correlation $R = -0.64$ for WB, $b = -0.73$ ($R = -0.58$) for CM and $b = -0.41$ ($R = -0.47$) for SH.

The displayed slant also explained most of the variance of the perceived tilt [Fig. 3(b)]: $F(8, 834) = 18.0$ ($P < 0.001$) for WB, $F(8,828) = 28.0$ ($P < 0.001$) for CM and $F(8, 820) = 58.9$ ($P < 0.001$) for SH. As was the case for the perceived slant, the perceived tilt was a decreasing function of the displayed slant.

The underestimate of the perceived slant also has been found when slant was estimated from the texture gradient instead of shading (*cf.* Perrone, 1982). However, the main

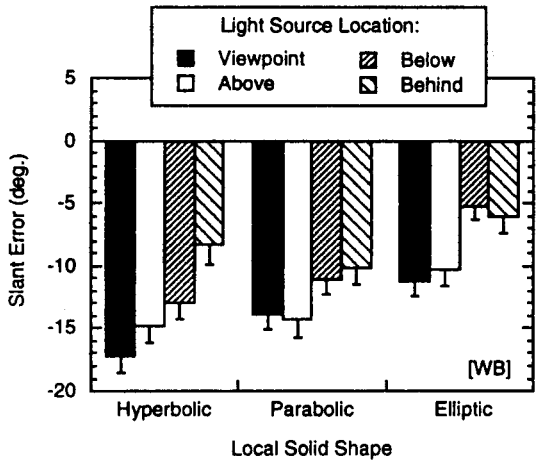

FIGURE 4. The effect of the local solid shape, and its interaction with the light source direction, is shown here for one subject.

effect of the displayed slant on the perceived tilt was unexpected. One explanation can nevertheless be advanced by re-examining the set of displayed points (Appendix A). Out of 36 measurement points, 30 were chosen within a small stripe on the surface (their displayed tilt was on the average 40 deg, SD 18.5 deg). The effect of displayed slant on perceived tilt can be interpreted, therefore, as a misperception of the overall orientation of this stripe, probably resulting from a misperception of the orientation of the whole object (*cf.* also Mingolla & Todd, 1986). This interpretation is reinforced by looking at the remaining six points for which the displayed tilt was chosen to be about 180 deg away from the others; for these points and for some subjects, the perceived slant and tilt appear to depart from the general decreasing trend (15 and 55 deg slants in Fig. 3). We shall return to this finding during the analysis of the second experiment.

Local solid shape. The variance in the settings which was not explained by the displayed slant variable was distributed between the remaining factors and interactions, namely the shape factor, the interaction between shape and displayed slant, and the illumination factor. All these factors and interactions were statistically significant at the 0.001 level, except for two conditions within the illumination variable (see next sub-section).

The shape variable characterizes the fact that the surface was locally hyperbolic, parabolic or elliptic at the measurement point. Among these three qualitatively different local shapes, elliptic points produced the smallest error in perceived slant (Fig. 4). When the data were pooled across displayed slants, illumination conditions and subjects, the means of the slant error were −6.64, −10.8 and −14.3 deg for elliptic, parabolic and hyperbolic points, respectively. This advantage for elliptic points could be the result of assuming *a priori* that the surface is locally spherical (*cf.* Pentland, 1984). We should note, however, that the larger error for hyperbolic points might be a result of the fact that mutual illuminations were not rendered on the surface. The ventral (hyperbolic) part on the croissant theoretically should, indeed, receive additional light from facing patches of the surface, whereas no surface patch faces the dorsal (elliptic) part of the croissant.

Another interesting observation can be made at the parabolic points. It can be shown that, at such a point, the isophote always has the same orientation, irrespective of the light source position (Koenderink & van Doorn, 1980; Blake *et al.*, 1985; Yuille, 1989; Mamassian, 1993). One implication of this property is the well-known appearance of a shaded cylinder, all of whose isophotes are oriented along its axis when the light source is reasonably far away. To appreciate the effect of the illumination condition on the perceived slant, we computed, for each measurement point, the SD of the slant errors across the illumination conditions. If the isophotes are used by our subjects, thus we should expect these SDs to be smaller for the parabolic points than for either the elliptic or hyperbolic points. There was indeed a trend in this direction: the averages across displayed slants and subjects of these SDs were 2.75, 3.26 and 3.33 deg for the parabolic, hyperbolic and elliptic points, respectively.

Light source direction. Out of six conditions (three subjects, two dependent variables), we found four cases in which the lighting factor was significant at the 0.001 level. The remaining two non-significant cases were found for subject CM for the slant variable, and for subject SH, for the tilt variable. Even when significant, the lighting factor explained the least, the amount of variance of any factor.

In the next section, we analyze further the effect of the illumination condition by computing the light source direction which is the most consistent with the observers' judgments. It is important to realize that none of the subjects was asked to report explicitly the direction of the light source, as was the case with previous experiments (Pentland, 1982; Todd & Mingolla, 1983; Mingolla & Todd, 1986). Indeed, it might be argued that the illumination is represented only implicitly by the visual system, in which case a verbal report or direct estimation could fail to be either accurate or consistent with the perceived shape. The computation of an implicitly assumed light source direction would enable us to test whether the visual system assumes a light source at an *a priori* position (e.g. above the scene, in between the object and the observer's head) or, at the opposite extreme, whether the visual system succeeds in accurately recovering the illumination condition used to render the scene.

IMPLICIT ILLUMINATION DIRECTION

Overview

From the local surface orientations reported by each observer in Experiment I, we can infer a hypothetical position of the light source for each of the illumination conditions. The idea is the following. Assuming a Lambertian reflectance model, the shading value at one

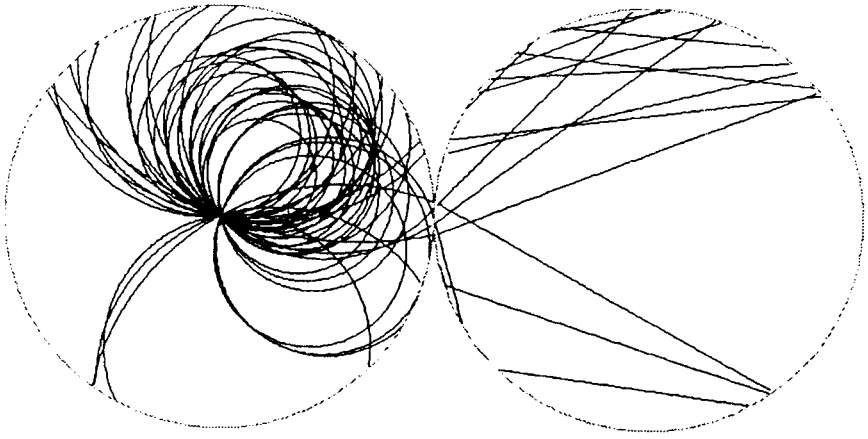

FIGURE 5. An assumed light source direction can be computed from the local orientation measurement as an intersection of constraints. The figure represents in stereographic projection the Gaussian sphere of the object, each disc representing one hemisphere (the direction of projection was chosen to be the true light source direction for the left disc, and the direction directly opposite for the right disc). Here, the constraining circles intersect at the true light source direction, simulating the behavior of an ideal estimator which knows the brightness and the surface orientation at each measurement point.

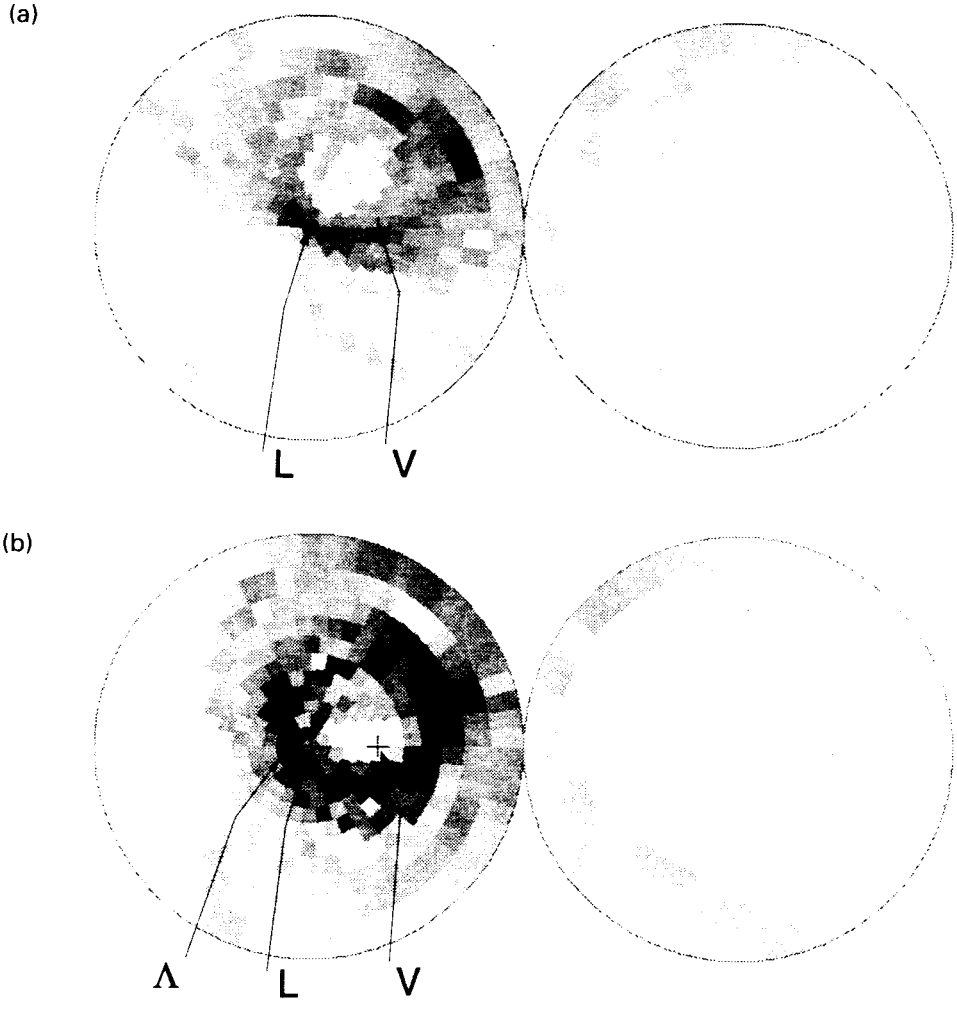

FIGURE 6. The assumed light source direction can be taken as the peak of the distribution obtained by binning the constraining circles. These distributions are shown here for the ideal estimator (a) and for subject WB (b), when the light source was located above the object. The center of the left disc corresponds to the true light source direction, while the eccentric cross corresponds to the viewing direction.

TABLE 1. Results of the implicitly assumed light source direction, expressed in (*slant*, *tilt*) relative to the viewing direction

	Viewpoint	Above	Below	Behind
Simulated	(0, 0)	(35, 120)	(65, −25)	(105, 60)
WB	(14, −75)	(49, 125)	(69, −168)	(100, 31)
CM	(21, −170)	(24, −52)	(73, −163)	(54, 167)
SH	(21, 130)	(25, −37)	(73, −151)	(95, 25)

point of the surface only depends on the orientation of the surface normal at that point relative to the light source direction [*cf. infra* equation (1)]. Conversely, if we know the brightness and the surface normal at one point, we can deduce the slant of the light source relative to this surface normal, without being able to say anything about the tilt. Each measurement point, along with its estimated local orientation, therefore provides one constraint on the direction of the light. The intersection of all the constraints supplied by the whole set of measurement points is then the light source direction most consistent with the observer's data.

Computations

The full formalization for the derivation of the assumed light source direction is provided in Appendix B. Since we are interested only in surface orientation, we can use the Gaussian sphere to represent the object. The Gaussian sphere is built by moving all the tails of the surface normals to the center of a unit sphere. From Lambert's law, each measurement then constrains the location of the light source to a circle on the Gaussian sphere. The center of this circle is the estimated normal to the surface at the measurement point and its radius is given by the incident angle at the point, which is in turn obtained from the inverse cosine of the brightness of the point. For display convenience, we project the Gaussian sphere onto a plane, using a stereographic mapping. We choose as the projection plane the tangent plane to the Gaussian sphere whose normal is the true light source direction. Through stereographic projection, each constraining circle for the light source maps to another circle on the projection plane. For an ideal observer, knowing precisely the brightness and the surface orientation at each measurement point, all these projected circles will intersect at one single point and this point corresponds to the implicitly assumed light source direction (Fig. 5). For the human observer however, these circles typically will not intersect at one single point because of the noisiness of the judgments. We can, nevertheless, build a distribution of the likelihood that the light comes from one particular direction (*cf.* Appendix B). The assumed light source direction is then taken to be the peak of this distribution (Fig. 6).

Results and discussion

The derived illumination models implicitly used by each of the three observers are shown in Table 1. For nine out of 12 implicit models (four light source directions, three subjects), the estimated slant of the light source direction was within 15 deg from the true light source. The largest slant departures were found when the light source was either at the viewpoint or behind the object. The tilt estimate of the light source direction (when the original was away from the viewing direction) was somewhat more variable. In particular, when the light source was below the object, the illumination models for the three observers also were located below the object, but on its left side instead of its right side. This result is interesting, because this symmetrically positioned light source would produce a radically different shading pattern on our simulated croissant (Fig. 7).

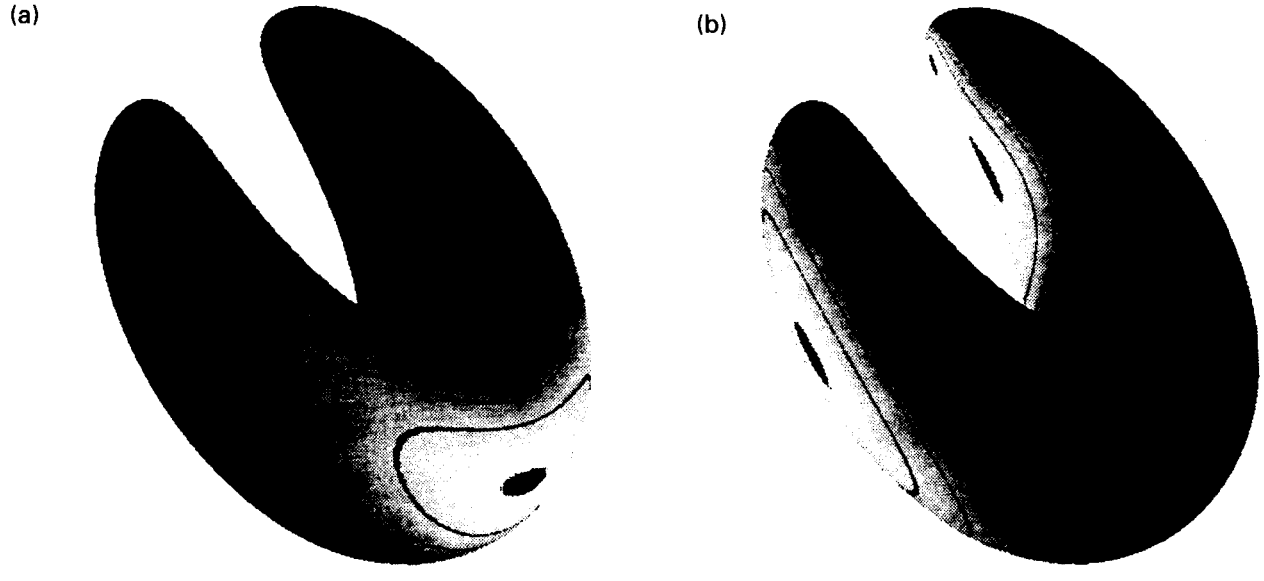

FIGURE 7. The isophotes on the surface of the object were dramatically different when the object was illuminated from (a) below [(*slant*, *tilt*) = (65 deg, −25 deg)] and from (b) the direction found to be the most consistent with the observer's settings for this condition [(*slant*, *tilt*) = (65 deg, −155 deg)].

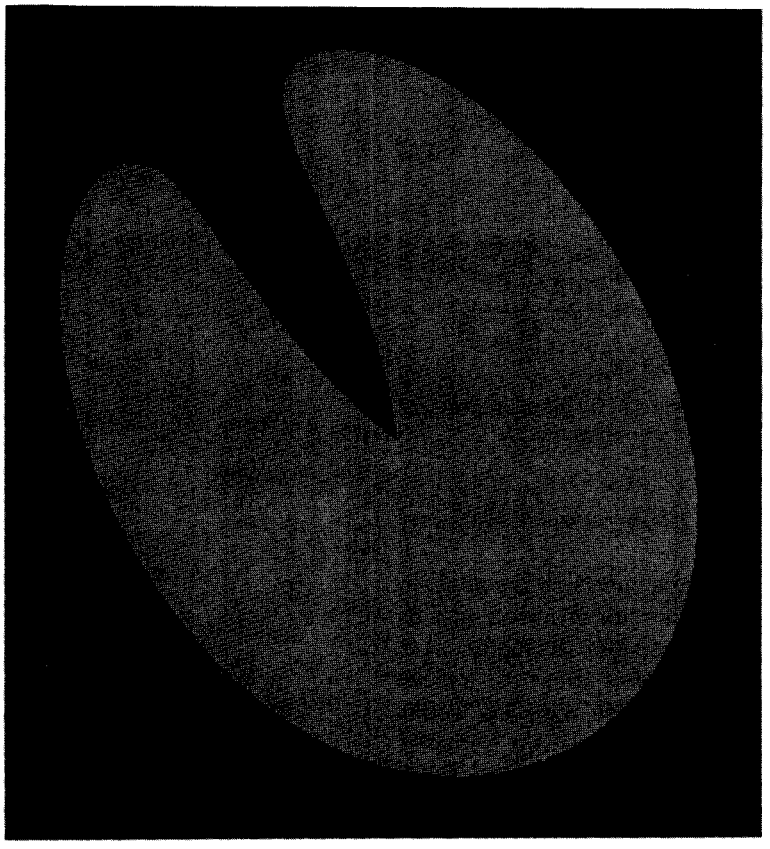

FIGURE 8. The object was displayed as a silhouette in the second experiment.

It is important to note that the estimate of the tilt of the light source was worse than the slant estimate. Indeed, the tilt of the illumination direction could be recovered directly from the image, for instance from the intersection of the attached shadow boundary with the occluding boundary. On the contrary, the slant component can be computed only if the object is assumed to be locally spherical at this intersection (Knill *et al.*, 1993).

Three possible interpretations emerge from the large error found for the assumed light source direction. In a first interpretation, the observer attempted to estimate the light source direction, but this estimate was not precise. As a result, the observer saw a different object from the one displayed and we should conclude that the visual system used an *inaccurate shape-from-shading* algorithm. In a second interpretation, the observer did not attempt to estimate the light source direction, but tried to use the shading information via some illuminant invariants such as the ones described by Koenderink and van Doorn (1980). Although these invariants provide a qualitative shape description, they appear insufficient to fully describe the object and therefore we shall refer to this interpretation as the *incomplete shape-from-shading*. In a final interpretation, the observer did not use the shading information at all, and estimated a three-dimensional shape from the occluding contour alone. We shall call this condition the *no shape-from-shading*.

We should note that in our three interpretations, the observers misperceived the object (in its global shape or orientation), an observation that we had already made while analyzing the perceived slant and tilt errors. In an attempt to investigate the validity of the *no shape-from-shading* interpretation for our stimulus, we designed a second psychophysical experiment in which the shading information was disrupted by displaying only the silhouette of the object.

EXPERIMENT II: SILHOUETTE

Methods

Subjects. Two subjects, naive to the purposes of the experiment, participated in this second study. The two observers (BS and FW) were graduate students familiar with computer-generated displays, only FW being a trained psychophysical observer. None of them had seen the full shaded croissant before running the experiment. All observers had normal, or corrected-to-normal vision.

Apparatus. The apparatus was identical to that used for the first experiment.

Stimulus. The object displayed was the same as in the first experiment, except that only the silhouette was now visible (Fig. 8). All shading variation was replaced by a uniform gray (55 cd/m^2) which clearly separated the object from the background (7.1 cd/m^2). The probe was unchanged.

Design. The same 36 points were selected from the surface, 12 in each of the three local solid shape

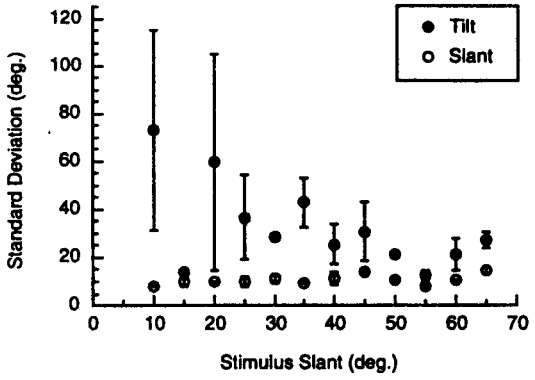

FIGURE 9. The SDs of the measurements for the second experiment were similar to the ones in the first experiment.

categories (*cf.* Appendix A). Eight repeated measures were recorded per point.

Subjects were instructed to "imagine that the contour was the silhouette of a three-dimensional object" and to match the surface orientation at the highlighted point as if this point lay on that object. Note that the object orientation was ambiguous, that is, the right half could be perceived either closer to or farther away from the observer (the main information to remove this ambiguity lies at the T-junction, which was replaced by an L-junction on the stimulus). To be able to compare the results of this experiment with the previous one, the subjects were told that the left half was closer.

Results and discussion

During a post-experiment interview, both subjects complained that the task was quite difficult, since the object did not appear three-dimensional. We ran the same data analysis as for the first experiment.

The reproducibility of the observer's measurements was similar in the first experiment to this second experiment (Fig. 9). More importantly, the decrease of the perceived slant and tilt as a function of the displayed slant were found again in this second experiment (Fig. 10). Therefore, the slant underestimation phenomenon described for the first experiment is not unique to the use of a Lambertian reflectance model. A similar conclusion was reached by Johnston and Passmore (1994b) who reported that observers were equally good in a geodesic alignment task, whether or not shading information was available.

In the first experiment, we found that two slants produced somewhat different responses for two out of three subjects. Here again in the second experiment, one of the subjects showed a different behavior when the displayed slant was 15 or 55 deg. This result provides further evidence that the observers misperceived the global orientation of the object. This global misorientation then seems to be driven purely by the occluding contour, since four different illumination conditions, and a fifth condition where the object was displayed as a silhouette, produced similar biases.

We now compare human performance with some

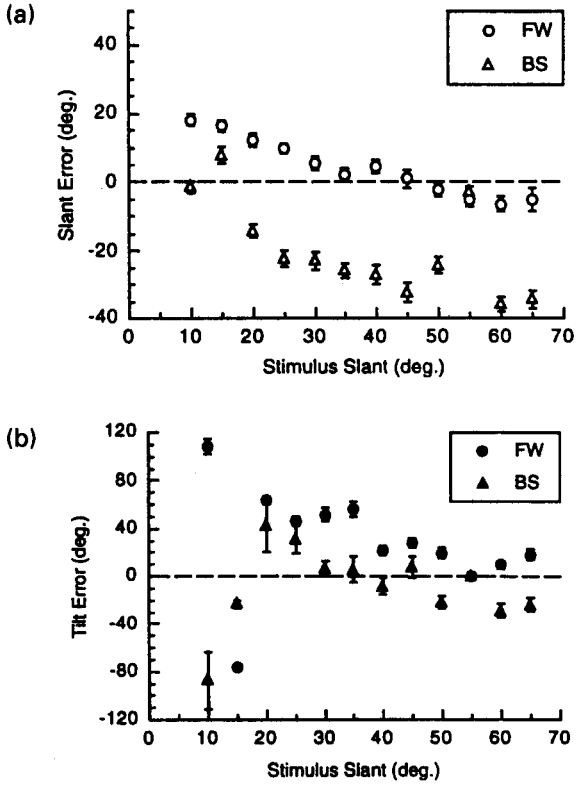

FIGURE 10. When the object was displayed as a silhouette, the perceived slant (a) and tilt (b) were again a decreasing function of the displayed slant for both subjects.

computer simulations of an algorithm which attempts to recover the surface orientation from the shading and occluding contour information. This comparison is an attempt to decide whether human performance is mostly attributable to a failure of the visual system to deal with these shaded images, or to the limited information provided by these images. For instance, the increasing underestimate of slant might be a property of the stimulus itself, in which case any shape-from-shading algorithm should show a similar bias.

COMPUTER SIMULATIONS

Overview

In this section, we present computer simulations of an algorithm which recovers the smoothest surface compatible with both the occluding contour and the pattern of shading within this contour. We have developed the algorithm with two criteria in mind, namely simplicity and psychological relevance (Mamassian, 1993). With respect to the first criterion, the classical work of Ikeuchi and Horn (1981) provided the main inspiration. Concerning the second criterion, we used slant and tilt as dependent variables to be able to compare the algorithm performance with the data collected in humans as described in the previous sections. The algorithm can be interpreted as finding the *a posteriori* most probable surface under the prior constraints assumed. In this sense, it is an ideal observer for shape estimation in that it is the *maximum a posteriori* Bayesian model for shape from

shading (Kersten, 1990; Knill & Kersten, 1990). No claim is made that our algorithm is the most up-to-date practical tool to recover shape from shading given a single image. For alternative methods, the interested reader is referred to Horn and Brooks (1989), Horn (1990), Pentland (1990) and Dupuis and Oliensis (1994).

Image formation. Before attempting to recover the shape of an object from its image, first we should make clear how this image is formed. For a small surface patch, the image irradiance is proportional to scene radiance and depends only on the incidence angle of the light and on the orientation of the patch relative to the viewer (Horn, 1986); the function which describes this relationship is here called the *reflectance map*. The reflectance map that we are considering in this paper corresponds to *Lambertian* surfaces which appear equally bright from any viewpoint. For such a surface, the irradiance is then proportional to the dot product between the light direction and the surface normal. In terms of slant σ and tilt τ of the surface normal, the Lambertian reflectance is:

$$R(\sigma, \tau) = \max\{\sin\sigma^*\sin\sigma\cos(\tau^* - \tau) + \cos\sigma^*\cos\sigma, 0\} \quad (1)$$

where (σ^*, τ^*) represents the direction of the light source (Mamassian, 1993). When the light source is located at the viewpoint ($\sigma^* = 0$), the reflectance map is independent of surface tilt [Fig. 11(a)]. Moving the light source away from the viewpoint deforms the reflectance map so that a maximum is created at the light source direction [Fig. 11(b)]. Rotating the light source about the viewing direction merely shifts the reflectance map along the surface tilt axis.

The Lambertian reflectance corresponds to perfectly smooth and matte surfaces, such as plaster or paper. Recently, a model which generalizes Lambertian reflectance has been proposed for rough matte surfaces, such as stoneware or concrete (Nayar & Oren, 1995; Oren & Nayar, 1995). The shading gradient on a rough surface is much reduced, as shown in Fig 11(c). For extremely rough surfaces, the image of an object reduces to its silhouette, as exemplified by the lack of shading on the full moon. This model can, therefore, be seen as providing a continuum between Lambertian reflectance and no shading at all.

For extended surfaces such as the whole object, several simplifying assumptions shall be added. We shall suppose first that the light source is sufficiently remote so as to assume that light has a constant intensity and direction of incidence on the surface. We shall suppose also that the object has uniform albedo. Finally, we shall neglect the effects of mutual illumination.

Regularization. We would like to solve the inverse optics problem so as to find a three-dimensional shape consistent with the image intensity values. We shall assume that the object has a Lambertian reflectance, and that the light source direction has been estimated by an independent method (e.g. Pentland, 1982). Locally this problem is ill-posed, because we are trying to recover a

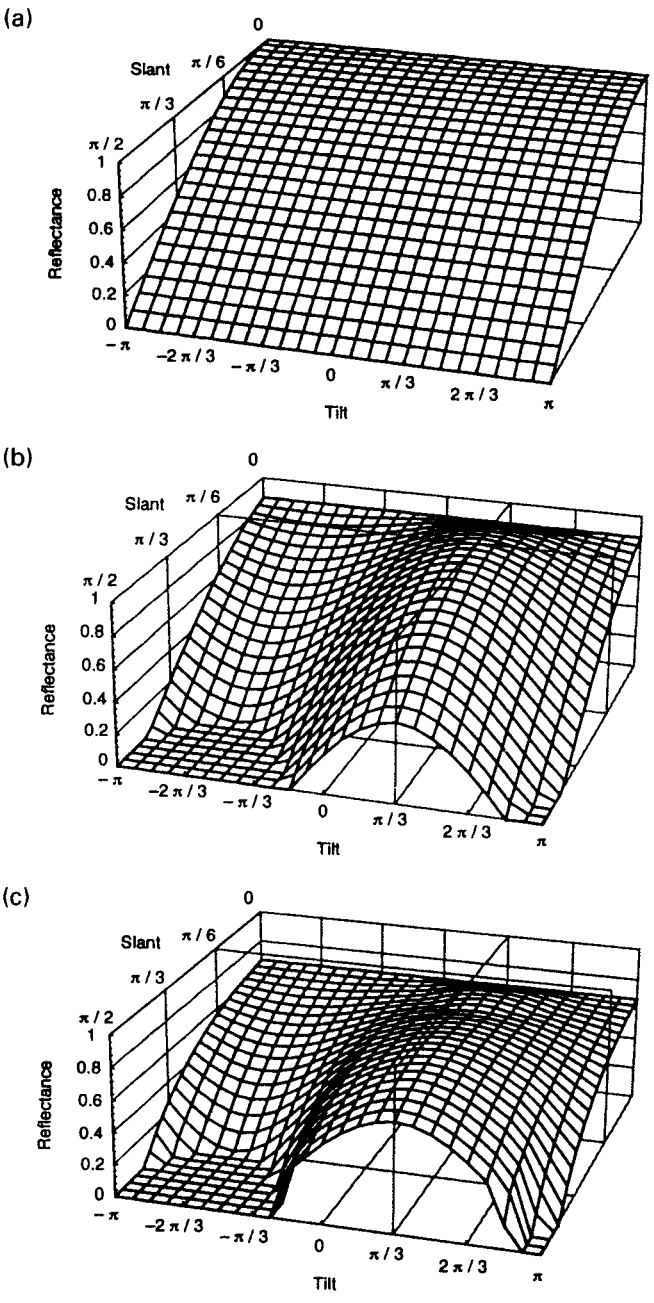

FIGURE 11. These plots show different reflectance maps as a function of slant and tilt of the surface normal at one point. (a) The Lambertian reflectance map when the light source is located at the viewpoint shows the classical cosine fall-off of image irradiance as a function of surface slant. (b) When the light source is moved away from the viewpoint (at a slant of $\pi/6$ and a tilt of $\pi/3$), the Lambertian reflectance reveals a maximum for that direction. (c) For a rough (non-Lambertian) reflectance, the irradiance in the light source direction is much reduced, while the irradiance at the occluding contour is increased [roughness index of Nayar and Oren (1995): σ = 30 deg].

variable with 2 d.f. (slant and tilt of the local surface orientation) from the image intensity which has only 1 d.f. However, by integrating the information over the whole surface, it can be shown that the global problem of reconstructing the entire object is well-posed over most parts of the image (Oliensis, 1991). Nevertheless, for better comparison with our psychophysical experiment in

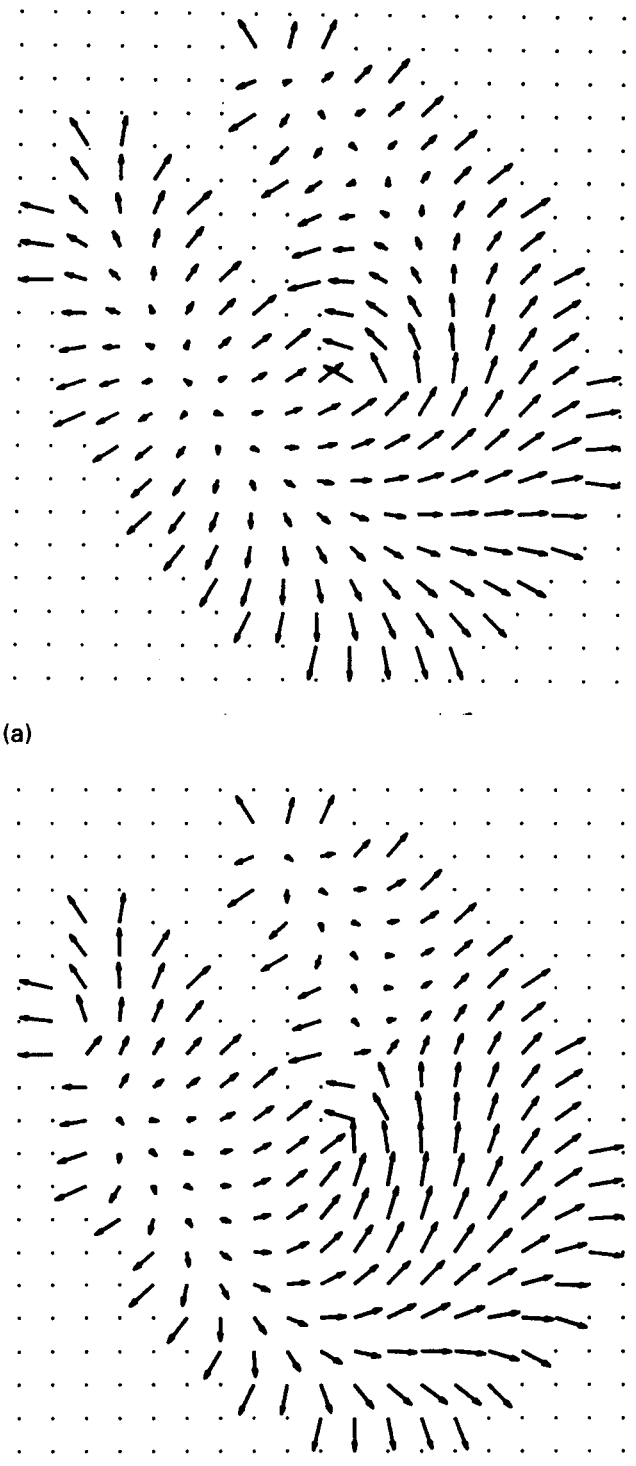

(a)

(b)

FIGURE 12. The shape estimated by the algorithm after 16 iterations (b) comes close to the displayed shape (a). Each plot shows the surface normal at regularly sampled points on the image of the surface (147 points total).

which the task was a local surface orientation matching, we shall follow the more traditional approach of imposing an additional constraint to render the problem well posed. This is the principle of *regularization* (Poggio *et al.*, 1985), in which the additional constraint is smoothness. The smoothness term can be identified with an explicit Bayesian prior model of shape. The model penalizes rapid changes in surface orientations, and attempts to minimize:

$$\int\int_{\Omega}\Big[(E(x,y)-R(\sigma,\tau))^2+\lambda((\sigma_x^2+\sigma_y^2)+(\tau_x^2+\tau_y^2))\Big]\,dxdy, \tag{2}$$

where the x and y subscripts indicate partial derivatives relative to x and y, respectively. The squared difference in the image formation term is equivalent to assuming Gaussian noise. The method to minimize such an integral is described in Mamassian (1993) and is based on a Gauss–Seidel relaxation scheme (Ikeuchi & Horn, 1981). This relaxation needs some boundary conditions to converge. The occluding contour provides a good candidate for the boundary conditions, since the surface orientation is known there.

By comparing the estimated shape reached at equilibrium with the original shape (Fig. 12), we can see that most of the error is concentrated near the cusp of the occluding contour. Probably a better shape estimate could have been obtained had we included the part of the occluding contour which overlaps the surface in the neighborhood of the T-junction (Fig. 1).

The smoothness constraint injected in the algorithm is weighted by a regularizing coefficient λ. If the value of this coefficient is zero, no smoothness is imposed and the surface constructed is based purely on the data available—i.e. the intensity values. If λ is infinite, the algorithm finds the smoothest surface consistent with the occluding contour. From repeated simulations with different values for the regularizing coefficient, we found that the surface recovered by the algorithm was the closest to the original surface (in terms of root mean square error) when λ was ≈ 1 [Fig. 13(a)]. With such a choice for λ, the algorithm converges in about 20 iterations.

Illumination direction. Our algorithm assumed that the position of the light source is known. We now look at how critical this assumption is. For this purpose, we ran our algorithm on the same image intensities, but with different assumed illumination directions, which were displaced from the true light direction by various amounts. We varied the angle between the true and assumed light source directions from 0 (no error) to 180 deg (a light source direction directly opposite to the one used to produce the image intensities). The results of these simulations are plotted in Fig. 13(b). For instance, an error of 135 deg in the direction of light produces a root mean square error on the computed surface orientation which is about five times the error obtained when the true light source direction is given. This result quantifies our statement above that a bad estimate of the light source direction produces a dramatic deformation of the recovered shape.

Slant and tilt errors. The performance of our algorithm can be directly compared with the results of our psychophysical experiments. After the algorithm stabilized on a surface, we computed the slant and tilt errors

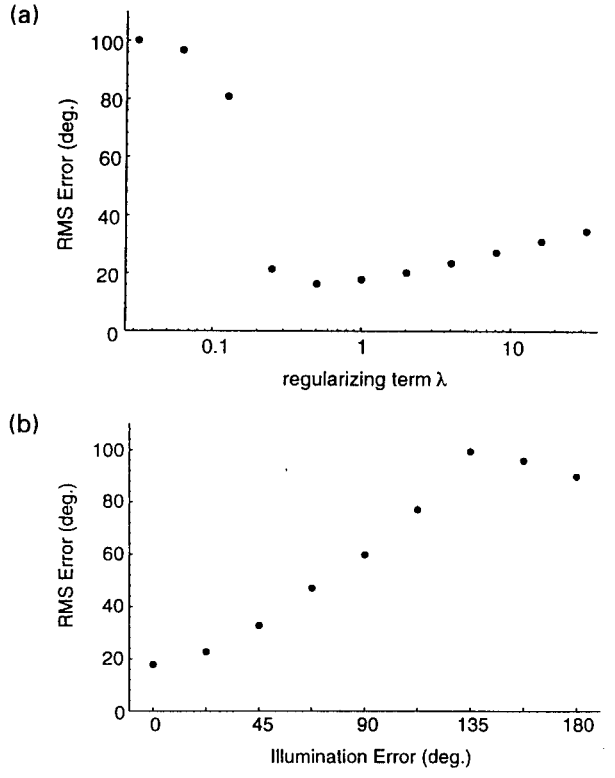

FIGURE 13. These plots show the influence of the regularizing term (a) and of the correctness of the assumed light direction (b) on the estimated shape.

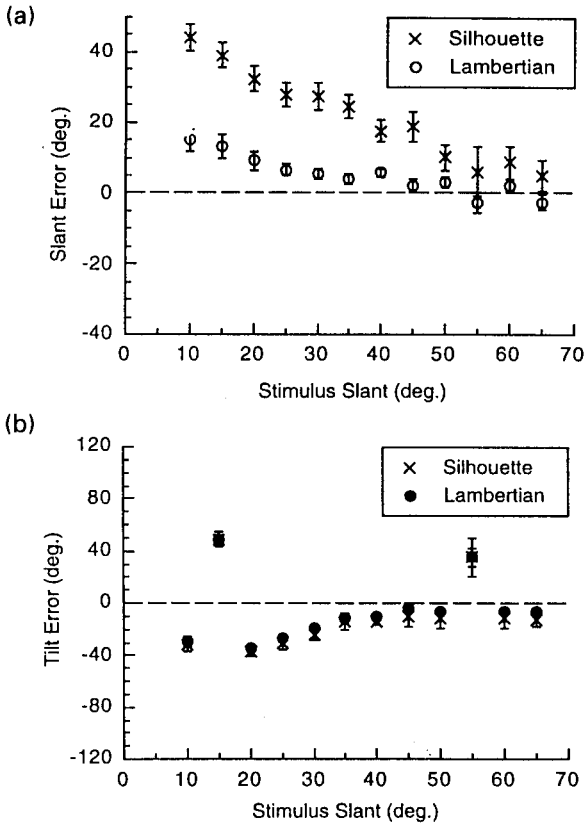

FIGURE 14. The performance of the algorithm is here shown in the same format as for the human observers in the psychophysical experiment. The use of the shading information by the algorithm substantially improved the estimated slant at the measurement points (a), but had a negligible effect on tilt (b). Error bars are SDs of the means obtained across local shape and illumination conditions.

for all 36 points used in the experiments by linear interpolation between the sampled points on the surface (Fig. 14). The simulations included all four illumination conditions of the first experiment (summarized here as the "Lambertian" conditions) and the case of the second experiment where the object was uniformly shaded (the "silhouette" condition). For the Lambertian conditions, the algorithm was given the correct light source direction and the regularizing factor was set to $\lambda = 1$; the silhouette condition was simulated by taking an infinite regularizing factor.

The computed tilts were identical in the Lambertian and silhouette conditions. The tilt errors were affected by the stimulus slant, but in the opposite direction than were the subjects in the psychophysical experiments. This tilt-reversal might be a consequence of the ambiguity regarding the orientation of the croissant (*cf.* design section of the silhouette experiment).

The computed slant was largely overestimated for small stimulus slants in the silhouette condition. This produced a negative slope of the slant error as a function of stimulus slant similar to what was found with all subjects in the two psychophysical experiments. In the Lambertian conditions, this slant effect was significantly attenuated. The similarity between the simulated silhouette condition and the performance of the human observers can be taken as further evidence that the subjects did not use the shading information, but instead derived a perceived shape from the occluding contour.

SUMMARY AND CONCLUSIONS

In the first experiment where we displayed a croissant-shaped object with Lambertian shading, we found a consistent underestimate of the slant by as much as 30 deg when the displayed slant was 60 deg. This underestimation of slant was similar in four drastically different illumination conditions.

To investigate further the effect of the illumination condition, we computed an assumed light source direction for each subject in each condition. In some cases, we found a large error in the tilt of this light direction, even though the tilt can *a priori* be determined easily from the image. This result led us to conclude that the illumination direction was probably not used by the observer to estimate the shape of the object, a conclusion also reached by Mingolla and Todd (1986).

In a second psychophysical experiment, we displayed only the silhouette of the same object. We found a similar decrease of the perceived slant as a function of displayed slant. On the other hand, computer simulations based on a Lambertian shape from shading algorithm did not produce such a biased reconstructed slant. Together with the weak effect of the illumination condition in the first psychophysical experiment, these results led us to

conclude that the occluding contour was overriding the shading cue in the observers' judgments. The ability to estimate local orientation away from the contour then may depend on either the use of *a priori* smoothness constraints (such as the one used in the algorithm), or on the ability to access knowledge about croissant-like shapes indexed by the contour.

The underestimate of slant found in both experiments still needs to be explained. One possibility is that the probe itself was misperceived. The underestimate of the judged slant could result from an overestimate of the depth of the probe (*cf.* Zimmerman *et al.*, 1995), or a flattening of the textured sphere which supported the probe. Although we tried to reduce such biases by introducing some practice trials with feedback in the experiment, such a possibility cannot be definitively ruled out. A second explanation for the slant underestimation is that the observers misperceived the global orientation of the object. That this might be the case is suggested from an unexpected effect of the displayed slant on the perceived tilt error.

The local solid shape of the surface (whether it was hyperbolic, parabolic, or elliptic) also had a significant effect on the perceived surface attitude. The result that elliptic patches led to less biased perceived slants could be interpreted as an indication that the visual system assumes a surface patch to be *a priori* elliptic. However, such a conclusion should be deferred until the slant underestimation is fully understood.

A final remark should be made concerning the choice of a Lambertian reflectance model to render the object in the main experiment. It is well known that Lambertian shading is an accurate model for only a limited number of surface materials. However, it appears that this model is also the one which provides the highest image contrast (Nayar & Oren, 1995). At the other end of the continuum for matte reflectance models lies the 'no-shading' case, where the object appears as a silhouette. We have tested experimentally both of these models (Lambertian and silhouette) on different subjects, and found similar results in terms of variability and bias. It seems that if shading was used in our experiment the observers would have been more accurate (less variable or less biased) for the Lambertian than for the silhouette experiment. Thus, from the results presented in this paper, there is no reason to expect human performance to improve with other reflectance models.

In comparison to the study of Mingolla and Todd (1986) who found some effect, although large inaccuracies, of shading for stimuli that had an identical elliptical occluding contour, we found here that shading had a negligible effect on perceived shape for our more complex occluding contour. While our observers complained that the silhouette of the object did not appear three-dimensional, their performance was not worse than those who could see the fully shaded object. Although intuition and introspection suggest that there is a shape component to the realism that shading provides, this component still awaits quantification.

REFERENCES

Ballard, D. H. & Brown, C. M. (1982). *Computer vision*. Englewood Cliffs, NJ: Prentice-Hall.

Berbaum, K., Bever, T. & Sup Chung, C. (1984). Extending the perception of shape from known to unknown shading. *Perception, 13*, 479–488.

Blake, A., Zisserman, A. & Knowles, G. (1985). Surface descriptions from stereo and shading. *Image & Vision Computing, 3*, 183–191.

Brewster, D. (1826). On the optical illusion of the conversion of cameos into intaglios and of intaglios into cameos, with an account of other analogous phenomena. *Edinburgh Journal of Science, 4*, 99–108.

Bülthoff, H. H. & Mallot, H. A. (1988). Integration of depth modules: Stereo and shading. *Journal of the Optical Society of America, A5*, 1749–1758.

do Carmo, M. P. (1976). *Differential geometry of curves and surfaces*. Englewood Cliffs, NJ: Prentice-Hall.

Cavanagh, P. & Leclerc, Y. G. (1989). Shape from shadows. *Journal of Experimental Psychology, Human Perception and Performance, 15*, 3–27.

Dupuis, P. & Oliensis, J. (1994). An optimal control formulation and related numerical methods for a problem in shape reconstruction. *The Annals of Applied Probability, 4*, 287–346.

Erens, R. G. F., Kappers, A. M. L. & Koenderink, J. J. (1993). Perception of local shape from shading. *Perception & Psychophysics, 54*, 145–157.

Foley, J. D., van Dam, A., Feiner, S. K., Hughes, J. F. (1990). *Computer graphics, principles and practice* (2nd edn). Reading, MA: Addison–Wesley Publishing Company, Inc.

Franz, E. & Growe, B. (1984). *Georges Seurat: Drawings*. Boston, MA: Little, Brown & Co.

Gibson, J. J. (1950). *The perception of the visual world*. Boston, MA: Houghton Mifflin Co.

Hilbert, D. & Cohn-Vossen, S. (1932). *Anschauliche geometrie* (English translation: *Geometry and the imagination*. New York: Chelsea, 1952 edn). Berlin: Springer.

Horn, B. K. P. (1986). *Robot vision*. Cambridge, MA: MIT Press.

Horn, B. K. P. (1990). Height and gradient from shading. *International Journal of Computer Vision, 5*, 37–75.

Horn, B. K. P. & Brooks, M. J. (1989). *Shape from shading*. Cambridge, MA: MIT Press.

Ikeuchi, K. & Horn, B. K. P. (1981). Numerical shape from shading and occluding boundaries. *Artificial Intelligence, 17*, 141–184.

Johnston, A. & Passmore, P. J. (1994a). Shape from shading. I: Surface curvature and orientation. *Perception, 23*, 169–189.

Johnston, A. & Passmore, P. J. (1994b). Shape from shading. II: Geodesic bisection and alignment. *Perception, 23*, 191–200.

Kersten, D. (1990). Statistical limits to image understanding. In Blakemore, C. (Ed.), *Vision: Coding and efficiency*. Cambridge, U.K.: Cambridge University Press.

Knill, D. C. & Kersten, D. (1990). Learning a near-optimal estimator for surface shape from shading. *Computer Vision, Graphics and Image Processing, 50*, 75–100.

Knill, D. C., Mamassian, P. & Kersten, D. (1993). The geometry of shadows (TR 93-47). Department of Computer Science, University of Minnesota.

Koenderink, J. J. (1990). *Solid shape*. Cambridge, MA: MIT Press.

Koenderink, J. J. & van Doorn, A. J. (1980). Photometric invariants related to solid shape. *Optica Acta, 27*, 981–996.

Koenderink, J. J., van Doorn, A. J. & Kappers, A. M. L. (1992). Surface perception in pictures. *Perception & Psychophysics, 52*, 487–496.

Lehky, S. R. & Sejnowski, T. J. (1990). Neural network model of visual cortex for the determining surface curvature from images of shaded surfaces. *Proceedings of the Royal Society of London, B240*, 251–278.

Mamassian, P. (1993). Isophotes on a smooth surface related to scene geometry. In Vemuri, B. C. (Ed.), *Geometric methods in computer vision II, Proceedings of SPIE, 2031*, 124–133.

Mamassian, P., Kersten, D. & Knill, D. C. (1996). Categorical local shape perception. *Perception*, in press.

Mingolla, E. & Todd, J. T. (1986). Perception of solid shape from shading. *Biological Cybernetics, 53*, 137–151.
Nayar, S. K. & Oren, M. (1995). Visual appearance of matte surfaces. *Science, 267*, 1153–1156.
Oliensis, J. (1991). Shape from shading as a partially well-constrained problem. *CVGIP: Imagine Processing, 54*, 163–183.
Oren, M. & Nayar, S. K. (1995). Generalization of the Lambertian model and its implications for machine vision. *International Journal of Computer Vision, 14*, 227–251.
Pentland, A. P. (1982). Finding the illuminant direction. *Journal of the Optical Society of America, 72*, 448–455.
Pentland, A. P. (1984). Local shading analysis. *IEEE Transactions on Pattern Analysis and Machine Intelligence, PAMI6*, 170–187.
Pentland, A. P. (1990). Linear shape from shading. *International Journal of Computer Vision, 4*, 153–162.
Perrone, J. A. (1982). Visual slant underestimation: a general model. *Perception, 11*, 641–654.
Poggio, T., Torre, V. & Koch, C. (1985). Computational vision and regularization theory. *Nature (London), 317*, 314–319.
Ramachandran, V. S. (1988). Perceiving shape from shading. *Scientific American, 259(2)*, 76–83.
Rider, P. R. (1942). *Plane and spherical trigonometry*. New York, NY: The Macmillan Co.
Stevens, K. A. (1983). Slant-tilt: The visual encoding of surface orientation. *Biological Cybernetics, 46*, 183–195.
Todd, J. T. & Mingolla, E. (1983). Perception of surface curvature and direction of illuminant from patterns of shading. *Journal of Experimental Psychology: Human Perception and Performance, 9*, 583–595.
Todd, J. T. & Reichel, F. D. (1989). Ordinal structure in the visual perception and cognition of smoothly curved surfaces. *Psychological Review, 96*, 643–657.
Yonas, A., Kuskowski, M. & Sternfels, S. (1979). The role of frames of reference in the development of responsiveness to shading information. *Child Development, 50*, 493–500.
Yuille, A. L. (1989). Zero crossings on lines of curvature. *Computer Vision, Graphics, and Image Processing, 45*, 68–87.
Zimmerman, G. L., Legge, G. E. & Cavanagh, P. (1995). Pictorial depth cues: A new slant. *Journal of the Optical Society of America, A12*, 17–26.

Acknowledgements—This research was supported by NSF BNS-9109514. Some of the results discussed in this paper were first presented at the Association for Research in Vision and Ophthalmology Annual Meeting in May 1993, in Sarasota, Florida. We thank Michael Landy and Peter Passmore for their comments on an earlier draft of the paper.

APPENDIX A

Selected Points for the Experiment

Table A1 gives the slant and tilt of the surface, relative to the observer, of the points where perceived surface orientation was measured.

TABLE A1.

Slant	Hyperbolic tilt	Parabolic tilt	Elliptic tilt
10.0	25.1	−6.5	10.2
15.0	−130.8	−114.9	−109.6
20.0	35.4	46.2	32.8
25.0	50.3	65.7	37.2
30.0	55.5	27.5	40.0
35.0	45.7	17.2	41.9
40.0	52.7	61.9	43.0
45.0	64.2	18.6	43.3
50.0	67.8	52.0	42.9
55.0	−169.5	−155.3	−139.9
60.0	49.5	59.6	36.1
65.0	56.7	21.7	39.8

For each of 12 slant values, three points were selected from the three local shape categories (elliptic, parabolic and hyperbolic). This table reproduces the tilts for each of these three points for a particular slant. Slant and tilt angles are in deg.

APPENDIX B

Illumination Constraints

From Lambert's law, each local surface orientation measurement constrains the location of the light source to a circle on the Gaussian sphere. The center of this circle is the estimated normal to the surface at the point where the measurement was made and its radius is given by the luminance at the point. The intersection of these circles can be interpreted as the light source direction implicitly assumed by the observer.

Since the Gaussian sphere is not convenient for display purposes, we shall map it onto a plane. Among the several ways to realize this mapping, we choose to use a stereographic projection because we are dealing exclusively with circles, and we know that the stereographic projection maps circles to circles (or straight lines) (Hilbert & Cohn-Vossen, 1932). Still we have to decide on the position of the origin of the plane of projection and its orientation. Since we are interested in recovering the illumination conditions, we will use the true light source direction as the origin (Fig. B1). Using such a mapping, every isophote on the surface will project to a circle centered at the origin. In particular, the attached shadow boundary will be a centered circle of radius 2. Finally, we orient the plane of projection such that the viewpoint will be located on the positive x-semi-axis of this plane.

Looking at the projected constraining circles discussed previously, we can appreciate immediately how good the observer's estimate of the light source direction is. This will be characterized by an intersection of the constraining circles closer or farther away from the center of the projection plane.

We shall denote by **V** the viewing direction, **L** the true light source direction (used to render the scene), **N** the surface normal at a measurement point and **M** the estimated surface normal (reported by the observer). Note that the illuminant direction is taken in the sense opposite to the light flow.

Each point on the Gaussian sphere is characterized by two coordinates, a latitude σ and a longitude τ. For instance, the position of one surface normal **N** relative to the light source direction **L** will be written as (σ_N^L, τ_N^L). Eventually we want to express the scene geometry relative to the true light source, since this will become the origin of our plane of projection.

The first element to compute is the incidence angle i, which is the angle between the illuminant direction **L** and the normal to the surface **N** (Fig. B2), using the notation that we have just introduced, $i = \sigma_N^L$. We need to express this angle as a function of the light source and normal positions relative to the viewpoint, since these are the ones that are available from the experiment. **L**, **N** and **V** are the vertices of a spherical triangle on the Gaussian sphere, whose edges are arcs of great circles. Applying the law of cosines for sides of spherical triangles (Rider, 1942), we obtain:

$$\cos i = \cos \sigma_N^L = \cos \sigma_L^V \cos \sigma_N^V + \sin \sigma_L^V \sin \sigma_N^V \cos (\tau_L^V - \tau_N^V), \quad \text{(B1)}$$

where (σ_L^V, τ_L^V) represent the slant and tilt of the light source direction, while (σ_N^V, τ_N^V) represent the slant and tilt of the surface normal at the point of measurement. For a Lambertian surface, the irradiance is directly proportional to the cosine of the incidence angle. Assuming that the product of the surface albedo by the light source intensity is one, this incidence angle will then be the radius of the constraining circle for the illuminant direction.

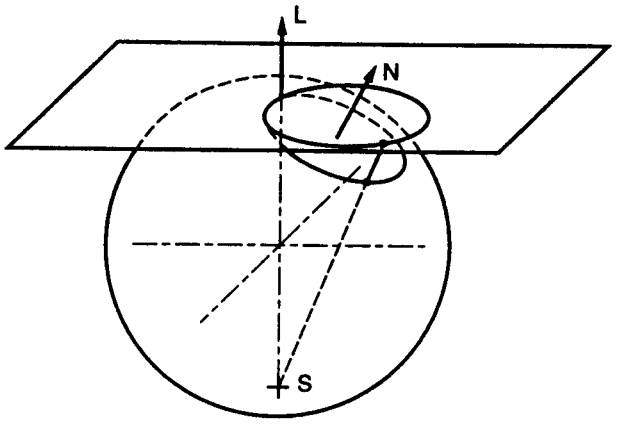

FIGURE B1. Under one illumination condition, each surface orientation measurement produces one constraining circle on the Gaussian sphere. This circle is mapped to another circle by stereographic projection, on the tangent plane to the Gaussian sphere at the true light source direction. The intersection of these constraining circles corresponds to the observer's assumed light source direction.

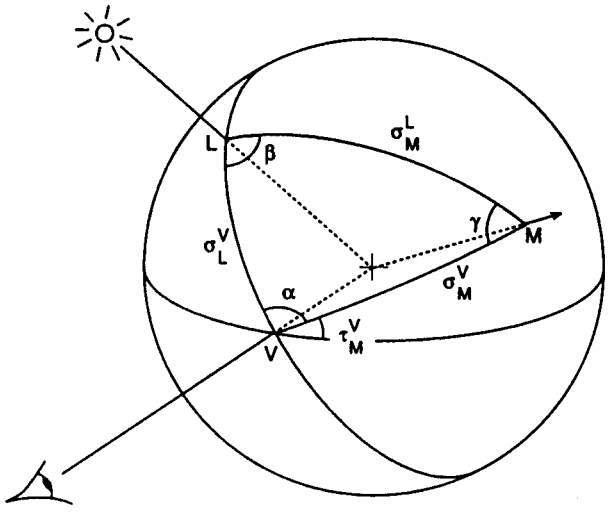

FIGURE B3. Geometry used to recover the latitude and longitude of the estimated surface normal relative to the illumination direction. **V**, **L**, and **M** represent the viewing, illumination and estimated surface normal directions, respectively.

We shall now compute the position of the estimated normal **M** relative to the illuminant direction **L**. **L**, **M** and **V** are the vertices of another spherical triangle on the Gaussian sphere (Fig. B3). We know two sides of this triangle, namely σ_L^V and σ_M^V, and the included angle $\alpha = \tau_L^V - \tau_M^V$. We can then use Napier's analogies to determine the remaining side σ_M^L and the two angles β and γ (we prefer to use Napier's analogies instead of the law of sines, since the former determines non-ambiguously the quadrant in which the angle falls; *cf.* Rider, 1942). The half-sum and difference of the unknown angles β and γ are given by:

$$\begin{aligned}\tan\frac{1}{2}\alpha\,\tan\frac{1}{2}(\gamma+\beta) &= \cos\frac{1}{2}(\sigma_L^V-\sigma_M^V)/\cos\frac{1}{2}(\sigma_L^V+\sigma_M^V)\\ \tan\frac{1}{2}\alpha\,\tan\frac{1}{2}(\gamma-\beta) &= \sin\frac{1}{2}(\sigma_L^V-\sigma_M^V)/\sin\frac{1}{2}(\sigma_L^V+\sigma_M^V)\end{aligned} \tag{B2}$$

This readily gives us β and γ. Now, since $\beta = \tau_M^L - \tau_V^L$, and given our choice $\tau_V^L = 0$ (we wanted the viewpoint to be located on the positive x-semi-axis of the projection plane), we can infer the longitude $\tau_M^L = \beta$. The latitude σ_M^L may then be found from either one of the following:

$$\begin{aligned}\tan\frac{1}{2}\sigma_M^L &= \tan\frac{1}{2}(\sigma_L^V+\sigma_M^V)\,\cos\frac{1}{2}(\gamma+\beta)/\cos\frac{1}{2}(\gamma-\beta)\\ \tan\frac{1}{2}\sigma_M^L &= \tan\frac{1}{2}(\sigma_L^V-\sigma_M^V)\,\sin\frac{1}{2}(\gamma+\beta)/\sin\frac{1}{2}(\gamma-\beta)\end{aligned} \tag{B3}$$

We now need to find the position of any point **P** on the constraining circle, whose center is **M** and radius i (Fig. B4). We can apply the same formulae as the ones previously derived, knowing the two sides σ_M^L and i, and the included angle α, which describes the polar-angle of our circle [varying over $[0, 2\pi)$]. Then we find the latitude σ_P^L and the longitude $\tau_P^L = \tau_M^L - \beta$.

Because of noise in the recovery process, all these computed circles will not intersect at a single point. To estimate the most likely illumination direction assumed by the observer, we shall use here a method similar to a Hough transform (Ballard & Brown, 1982). We tessellate the Gaussian sphere in spherical coordinates, so that each cell covers an equal area. As an index for the cell, we take the latitude and

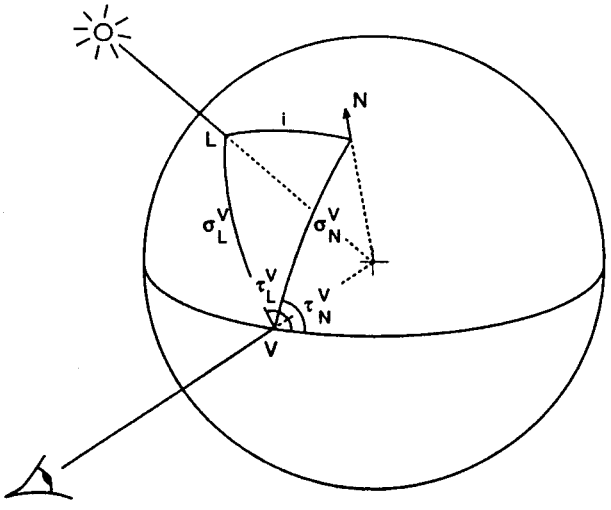

FIGURE B2. Geometry used to compute the incidence angle i. **V**, **L** and **N** represent the viewing, illumination and surface normal directions, respectively. These three vectors form a spherical triangle on the Gaussian sphere.

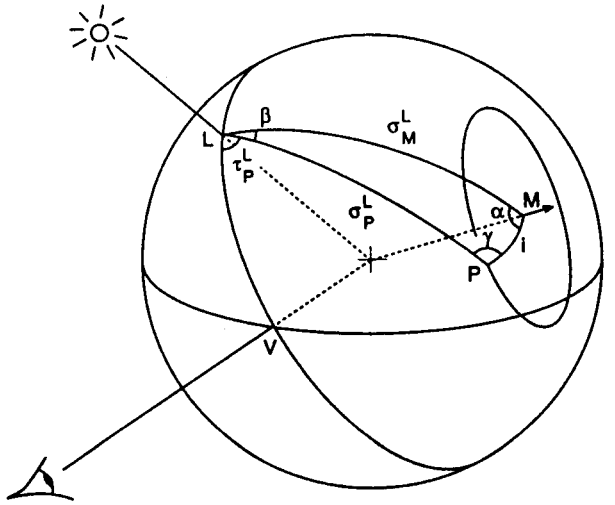

FIGURE B4. Spherical triangle used to recover the latitude and longitude of a running point on the circle constraining the position of the estimated light source.

longitude of the cell's center. Each constraining circle on the sphere is then approximated by n points and we increment every cell which is overlapped by one such point. Repeating this procedure for each constraining circle, we obtain a discrete approximation of the distribution of the estimated illumination direction. We choose the peak of this distribution for the observer's illuminant direction Λ.

We now map the Gaussian sphere on the tangent plane at the illuminant direction $\mathbf{L}$, using stereographic projection. We want to project each point $\mathbf{P}$ given by its latitude and longitude (σ_P^L, τ_P^L) into a point in the tangent plane described by its polar coordinates (r, θ). We obtain the following mapping:

$$\begin{aligned} r &= 2\tan(\sigma_P^L/2) \qquad \text{for } \sigma_P^L \in [0, \pi) \\ \theta &= \tau_P^L \qquad\qquad\quad \text{for } \tau_P^L \in [-\pi, \pi). \end{aligned} \tag{B4}$$